# Development and Evaluation of an Experimental Platform for State-of-Charge Balancing Control of Lithium-Ion Battery Systems

---

A

Thesis

Presented to

the faculty of the School of Engineering and Applied Science

University of Virginia

---

in partial fulfillment

of the requirements for the degree

Master of Science

by

Jiaao Wang

May 2024

# APPROVAL SHEET

This

Thesis

is submitted in partial fulfillment of the requirements
for the degree of

Master of Science

Author: Jiaao Wang

This Thesis has been read and approved by the examing committee:

Advisor: Zongli Lin

Advisor:

Committee Member: Nikhil Shukla

Committee Member: Qing Chang

Committee Member:

Committee Member:

Committee Member:

Committee Member:

Accepted for the School of Engineering and Applied Science:

Jennifer L. West, School of Engineering and Applied Science

May 2024

# Acknowledgments

I would like to extend my deepest gratitude to the Charles L. Brown Department of Electrical and Computer Engineering at the University of Virginia for unwavering support and invaluable resources throughout my journey in the Master's program. The department has not only provided me with an exceptional academic environment but also the opportunity to explore and grow both professionally and personally.

My heartfelt thanks go to my parents, who have been my cornerstone and my source of strength and inspiration. Without their sacrifices, love, and guidance, I would not be where I am today. Their belief in my abilities has been the driving force behind my accomplishments, and for that, I am eternally grateful.

I am particularly thankful to Professor Lin, who has been an extraordinary mentor and advisor. Professor Lin's expertise, patience, and guidance have been crucial in steering this thesis towards its completion. His encouragement and support have made a significant impact on my research and academic growth.

I would also like to express my gratitude to my research collaborators, Yangyang Qian and Carson Chase, for their invaluable contributions, insights, and camaraderie throughout this project. Working alongside them has been an immensely rewarding experience, and their assistance has been essential in the success of our research endeavors.

This journey would not have been possible without the collective support and encouragement of everyone mentioned, and for that, I am profoundly thankful.

# Abstract

State-of-charge (SOC) balancing has been the target of numerous battery management system (BMS) algorithms that have been put forth. The creation and assessment of an experimental platform for BMS algorithm testing are described in this thesis. Our designed platform facilitates simple parameter or physical amount expression adjustments, which makes evaluating the performances of different BMS algorithms more straightforward. The DSP processor (TMS320F28335), a specially made buck converter, different battery packs, and load resistors make up the platform's hardware. An SOC vs open-circuit voltage graph is generated for the purpose of estimating SOC by modeling circuit processes and examining battery output under load. The platform evaluation selects A BMS algorithm is adopted for the evaluation of the platform, confirming the efficacy of the algorithm in achieving SOC balancing across battery units.

# Contents

# List of Tables

# List of Figures

# Acronyms

**EES** Electrical Energy Storage. 1

**RES** Renewable Energy Source. 2

**BESS** Battery Energy Storage System. 3

**SCUC** Security-constrained Unit Commitment. 4

**BES** Battery Energy Storage. 5

**PV** Photovolta. 6

**LIB** Lithium-ion Battery. 7

**EV** Electric Vehicle. 8

**LPB** Lithium Polymer Batterie. 9

**BMS** Battery Management System. 10

**SOC** State of Charge. 11

**SOH** State of Health. 12

**DSP** Digital Signal Processing. 13

**DC-ES** Direct Current Electric Springs. 14

**PI** Proportional-Integra. 15

**OCV** Open-Circuit Voltage. 16

**EPWM** Enhanced Pulse Width Modulator. 17

# Chapter 1

# Introduction

## 1.1 Literature Review

Converting electrical energy from the grid into a form that can be stored and then converted back into electrical energy as needed is known as Electrical Energy Storage (EES) [1, 2]. When using intermittent energy sources or in times of low demand and low generation costs, this capacity allows the creation of power, which may then be used in times of high demand, high generation costs, or in the absence of other generating choices [3].

The attributes of energy storage, particularly its energy transfer efficiency and rapid ramp-up capabilities, have spurred interest in battery technologies to support the integration of renewable energy sources (RESs). The drive towards energy storage technologies has been fueled by the necessity to accommodate higher penetrations of RES, aiming to diminish the costs associated with meeting peak demand. Energy storage facilitates the shifting of energy from times of peak to off-peak demand, or the absorption of surplus renewable energy for later use, thereby enhancing grid stability. Furthermore, energy storage is positioned as a workable countermeasure to the

unpredictability and inconsistency of RESs because to its quick ramp-up capability. Utilizing energy storage can mitigate the operational strain on thermal power units, which typically are not designed for frequent load variations [4].

RESs are now essential to maintaining the viability of contemporary power supply systems in the face of growing worries about climate change, the burning of fossil fuels, and the need for a more sustainable grid architecture [5]. The surge in RESs integration has complicated the management of power system generation and demand equilibrium. Recent studies have explored the challenges associated with energy storage scheduling and its diverse applications in systems enriched with renewable resources. The studies in [6, 7] have assessed the role of wind energy in energy storage systems, employing a unit commitment model that accommodates the uncertainty of wind power generation. Moreover, the effect of erratic wind predictions on the energy storage system (pumped storage) valuation has been studied. A novel, system-wide methodology has been proposed to evaluate the contribution of grid-scale electric storage, optimizing investments across new generation capacities, network expansion, and storage capabilities, all while minimizing operational costs and adhering to reserve and security standards [8].

Batteries are one of the many storage technologies that provide a particularly promising way to manage the intermittent nature of RESs [9]. Batteries have no no-load costs and are often not constrained by minimum power input/output levels during the charging and discharging operations, in contrast to thermal power units. Batteries are positioned favorably within the range of energy storage options due to this benefit and their higher power density when compared to other energy storage technologies like compressed air energy storage and pumped hydro storage. Nonetheless, the principal obstacle to widespread adoption of battery technology remains its high initial investment cost. However, concerted efforts are currently underway to

mitigate these capital expenditures and enhance the cost-efficiency of various battery technologies [10].

Battery energy storage systems (BESSs) are crucial for enhancing the integration of renewable energy sources, such as solar and wind power, into smart grids. By storing excess energy generated at peak production times and releasing it during periods of high demand or low production, BESSs help to balance supply and demand, improving the stability and dependability of the power grid [11, 12].

Rechargeable batteries represent the most traditional method of electrical energy storage, converting electrical energy into chemical energy [1]. One or more electrochemical cells, each with a positive (anode) and a negative (cathode) electrode, together with an electrolyte in liquid, paste, or solid form, make up a battery. Reversible electrochemical reactions occur at both electrodes during the discharge process, which facilitates the flow of electrons across an external circuit. Because of its reversibility, the battery may be recharged by passing an external voltage across its electrodes.

Batteries improve system stability by responding quickly to changes in load and by incorporating external or co-generated power. Notably, batteries exhibit minimal standby losses and boast high energy efficiencies, ranging from 60% to 95%. Attributes such as short lead times, ease of installation, and technological modularity support the deployment of rechargeable batteries [13].

Large-scale battery storage has historically been hampered by issues including poor energy and power densities, high maintenance costs, short cycle lifetimes, and constrained discharge capacities. Additionally, the environmental impact of battery disposal is a critical consideration, given the toxic substances many batteries contain [14].

At the transmission and distribution system levels, battery storage applications have undergone extensive evaluation. Research has highlighted the benefits of batter-

ies within renewable energy transmission systems through security-constrained unit commitment (SCUC) modeling, examining the composition and scheduling of power systems with varying degrees of wind energy integration and the inclusion of battery energy storage (BES) as a viable energy storage solution [15, 16]. Using Lagrangian relaxation-based optimization algorithms, these studies have tackled the short-term battery scheduling in SCUC environments and investigated the intricate operational dynamics of PV/battery systems. They have also determined the hourly charging and discharging schedules of batteries linked to the utility grid. Moreover, investigations into grid-connected PV/battery systems have shed light on their influence on spot pricing, peak demand management, and transmission congestion [16].

At the distributed level, battery storage remains a pivotal area of research. A notable study delineated a three-step methodology for optimizing generation scheduling within islanded microgrids, focusing on initial thermal unit combination solutions, resolving thermal unit combination dilemmas, and optimizing renewable energy dispatch based on thermal unit commitment outcomes [17]. A novel strategy that makes use of cost-benefit analysis has also been put out to maximize the size of energy storage systems in microgrids while emphasizing the workings of lithium-based batteries during cycles of charging and discharging [18].

Of these battery kinds, lithium-ion battery systems are the most sought-after due to their high energy density, long lifespan, high voltage capacity, and low self-discharge rate [19]. These qualities also make them perfect for grid storage, electric cars, and portable electronics [20–22].

About thirty years ago, Sony was the first company to commercialize lithium-ion batteries (LIBs), a breakthrough that completely changed the portable electronics market and spurred a wave of interest in research [23]. The development of lithium-ion rechargeable batteries has been identified as a critical growth sector due to the

batteries' versatility, which can power anything from small electronic devices to large power storage systems and electric vehicles (EVs). Notably, these batteries are characterized by their compact size, ability to undergo stable cycling for more than 500 cycles, and their adaptability to a wide range of sizes—from microns to large batteries capable of energizing computer memory chips, communication devices, electronic displays, and EVs [24].

When it comes to specific capacity (3861 mAh $g^{-1}$), lithium metal stands out as the best option for the negative electrode in rechargeable batteries due to its high electronegativity and lowest density among metals [25]. Lithiated metal oxides, such as $LiCoO_2$, $LiMnO_2$, and $LiNiO_2$, are often used as cathodes in lithium-ion batteries (LIBs), whereas graphitic carbon, with its layered structure, is the most common anode material [26]. The introduction of LIBs transformed portable electrical design and made it possible for a wide range of handheld gadgets that are essential to modern living to proliferate.

Even though the initial composition of the cathode was basically unaltered, further advancements in LIB performance after commercialization were mostly focused on improving the energy densities, discharge/charge rates, and cycle lifetimes through adjustments to the anode and electrolyte components. Three different types of materials were found in Dahn's 1995 research on carbon anodes: hard carbon, graphite, and carbon containing hydrogen [27]. The substantial overpotential during delithiation has restricted the practical use of carbon materials containing hydrogen, despite their high capacity. Although graphite offered high capacity, its recyclability was a concern, leaving hard carbon as a viable alternative despite its disadvantages. By the mid-1990s, the market had largely transitioned to graphite anodes, with hard carbon's share diminishing significantly by 2010 [28].

Towards the late 20th century, the industry began shifting from liquid electrolyte

batteries encased in metal to lithium polymer batteries (LPBs) housed in plastic casings [29]. Central to LPB technology is the electrolyte's composition, ideally a solid-state polymer film mixed with a lithium salt. However, the operational temperature constraints of solid-state LPBs (60°C) led to the development of gel electrolytes as a hybrid solution, balancing the properties of solid and liquid electrolytes and offering cost and safety advantages due to reduced flammability risks [30].

Li-ion batteries have not only maintained their dominance in consumer electronics but have also expanded into the electric vehicle and uninterruptible power supply markets, incorporating advanced cathode technologies like spinel $LiMn_2O_4$ and olivine $LiFePO_4$ [31]. Research continues to explore next-generation Li-ion technologies, such as lithium- and manganese-rich anodes [32], 5V anodes [33], and silicon anodes, aiming for breakthroughs in cost and energy density. This ongoing research, traversing diverse subdisciplines within materials science and electrochemistry, seeks to enhance battery performance through both crystal structure optimization and morphological innovations.

Battery Management Systems (BMS) play a critical role in managing and guaranteeing the security of battery packs in applications that use lithium-ion batteries [34]. BMS's main responsibility is to enable the safe and dependable functioning of batteries by performing tasks like cell balance, charge regulation, and condition monitoring and assessment. Given the variability in battery performance due to operating and environmental conditions, BMS must accurately reflect the battery's status in terms of safety, usage, performance, and lifetime. Lithium-ion batteries pose risks of fire if overcharged, owing to their volatility and flammability, which is particularly concerning in electric and hybrid vehicles where such incidents can result in catastrophic outcomes [35]. Moreover, over-discharging can cause irreversible capacity loss due to chemical reactions. To mitigate these risks, BMS monitors and manages battery op-

eration through safety circuits, executing corrective actions upon detecting anomalies like overvoltage or overheating.

A well-designed BMS encompasses features for data acquisition, safety, status determination and prediction, charge/discharge control, battery balancing, thermal management, and communication with battery components and users, thereby extending battery life. From a hardware perspective, BMS implementations can adopt centralized, distributed, or modular architectures, each with similar functional objectives [36]. Challenges in BMS development, especially for electric vehicles, stem from complexities in assessing battery states, modeling, and balancing [37].

It is vital to comprehend battery states, such as State of Charge (SOC) and State of Health (SOH), in order to guarantee operational safety and dependability as well as to inform the charging and discharging procedures that are necessary for stable battery conditions. SOC, analogous to a fuel gauge, is challenging to estimate accurately due to factors like aging, environmental changes, and cycling, whereas SOH indicates the remaining battery life [38]. Battery modeling complicates further with the need to account for diverse electrochemical mechanisms, necessitating various equivalent circuit models to satisfy different material properties and accuracy requirements [39]. Battery degradation models aim to support SOH estimation but must consider dynamic external factors like ambient temperature and load currents [40].

Batteries in electric and hybrid cars are arranged in parallel and series configurations to satisfy precise voltage and capacity specifications. Variability among cells leads to uneven charging and discharging, risking overcharge or overdischarge in individual cells and potentially shortening the battery pack's lifespan. Effective cell balancing mechanisms are thus critical for maintaining uniform SOC levels across cells, minimizing disparities and prolonging battery life [41].

Evaluating battery state poses significant challenges but is vital for BMS perfor-

mance. Accurate SOC modeling is hindered by the nonlinear nature of lithium-ion batteries, influenced by varying scales and aging processes, and is further complicated by the internal and external environmental fluctuations [42]. Discrepancies in battery manufacturing affect pack performance, underscoring the need for reliable SOC monitoring techniques [43].

Coulomb counting, which integrates the current over time, and lookup tables, which connect certain parameters with SOC, are two techniques for estimating SOC. Both approaches have drawbacks, such as the requirement for routine calibration and the reliance on the correctness of the reference data [44]. The simplest technique for estimating SOC is coulometric counting, which measures a battery's energy in coulombs. By integrating the current entering and leaving the battery over time, this approach determines the capacity of a battery. At full charge, the SOC is determined by referring to a calibration point; however, because of battery age and coulombic efficiency, this reference point, or the starting point, may vary. Consequently, while running in real-world settings, the reference point needs to be adjusted, and the SOC estimate needs to be updated at various observed voltages [44]. Look-up tables are particularly helpful and simple to use; they map the relationship between the SOC characteristic parameters and the LIB, enabling for SOC estimate. The primary drawback of look-up tables is that they require the LIB to be kept standing for an extended amount of time in order to guarantee the accuracy of the measurements and the dependability of the internal electrochemistry. The precision of the tables employed also has a significant impact on the efficiency of SOC computations [45]. These methods show how continuous attempts are being made to improve SOC estimate, which is essential for efficient BMS operation and battery maintenance plans.

Several works have shown encouraging simulation results and empirically confirmed that SOC balancing control techniques are feasible. Creating a broad experi-

mental platform for battery systems is our goal in this project. The purpose of this platform is to enable the testing and validation of sophisticated SOC balance control algorithms, as those in [46, 47], that have been recently proposed for BESSs.

A prototype system was constructed to validate the proposed energy sharing controller for balancing the state-of-charge (SOC) in distributed battery energy storage systems. The prototype comprised two 18650 lithium-ion battery cells, two bidirectional dc-dc buck/boost power converters, and a programmable electronic load, all controlled by a TMS320F28335 microcontroller from Texas Instruments. This setup was used to simulate a small-scale version of the proposed system [48]. The SOC of the batteries was estimated using a coulomb-counting method, integrating current flow in and out of the batteries without the need for detailed battery modeling. The SOC values were updated by the controller every second, optimizing the balance between accuracy and speed of SOC balancing. The power converters were controlled by the microcontroller's PWM module, which adjusted the duty cycles based on SOC measurements. This thesis emphasizes the practical application of the proposed energy sharing controller, highlighting its feasibility and effectiveness in managing SOC balancing and dc bus voltage regulation in a real-world scenario.

A great example of combining the power of microcontrollers and digital signal processors (DSPs) into one chip is Texas Instruments' TMS320F28335 DSP, which provides strong performance for a range of high-demand applications [49]. Thanks to its floating-point capabilities and effective operation in intricate control algorithms, this integration makes it the perfect solution for applications demanding high performance, such as intelligent instrumentation, motor servo control, power electronics, and industrial automation. The 32-bit floating-point DSP core of the TMS320F28335 operates at a primary frequency of 150MHz, making it particularly effective at handling computationally demanding tasks. This processor is capable of

32*32-bit multiply-accumulate operations in a single cycle, an accomplishment that would require more than four cycles for a typical 32-bit microcontroller.

From a hardware standpoint, the F28335 has a large number of on-chip peripherals. These consist of a 12-bit AD converter with 16 analog input channels, 6 improved capture (CAP) units, 2 quadrature encoder pulse (QEP) units, 18 PWM channels, 6 of which are high-resolution PWM (HRPWM) channels, and an extensive set of communication interfaces (SCI, CAN, SPI, I2C). By enabling the creation of complicated control systems without the need for extra external components, this wide range of peripherals helps to reduce system complexity and costs [50]. TMS320F28335 DSP embodies a powerful blend of DSP and microcontroller features, offering a versatile platform for developing advanced digital control systems.

Converters are also a key component of the BMS test platform's structure. Converters plays a pivotal role in managing the interaction between energy storage units and the DC microgrid. Converters in the ESS architecture play a crucial role in enabling bidirectional power flow, allowing for both charging and discharging of the storage units. This bidirectionality is essential for smoothing out the intermittent output from renewable sources, facilitating intentional islanding during faults, and executing optimization routines for improved microgrid performance. The thesis describes the static V-I (Voltage-Current) characteristics of the ESU converters, illustrating their behavior under various load conditions and the impact of SOC balancing on their performance. The converters are designed to operate within specific current limits to prevent overcharging or excessive discharge, with these limits being dynamically adjusted based on SOC levels and system requirements [51].

The thesis elaborates on the implementation of a distributed cooperative control framework that includes primary and secondary control levels among DC-ESs within a DC microgrid. The thesis discusses the control mechanisms that involve converters

in the broader context of maintaining voltage regulation and power quality within DC microgrids. It emphasizes the importance of converters in facilitating the operation of DC-ESs, which are crucial for mitigating power imbalance and enhancing voltage quality. The primary control utilizes a droop mechanism for the coordination of multiple DC-ESs' operations, whereas the secondary control employs a consensus algorithm for adjusting the DC-bus voltage reference based on the state-of-charge (SOC) balance among DC-ESs. This hierarchical control scheme is essential for achieving efficient power distribution and stabilization within the microgrid, underlining the critical role of converters in this process [52].

## 1.2 Thesis Structure

Fig. 1.1 depicts a schematic diagram of our experimental platform, wherein each battery system consists of a battery unit and a power converter. Every battery unit generates power via a programmable buck converter, and the output voltage, current, or power of the battery is controlled by a DSP processor. Circuit operations are represented within the platform by using an external load resistor in conjunction with the electrical equivalent circuit model from [53]. The SOC of each battery unit can be estimated using this representation, which is described as a relationship with the open-circuit voltage [54]. The open-circuit voltage (OCV) is estimated in real-time during the experiment, acknowledging that each cell exhibits a distinct OCV and SOC relationship.

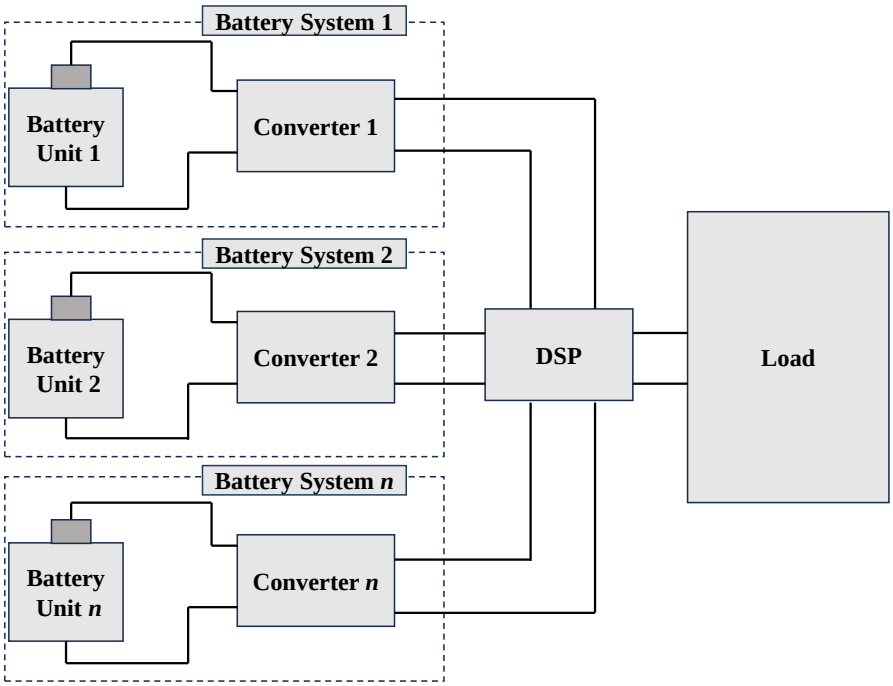


Figure 1.1: Schematic diagram of the experimental platform.

In the subsequent phases of our investigation, we delve into a comprehensive

evaluation and development narrative of an experimental platform designed for the meticulous study of State-of-Charge (SOC) balancing within lithium-ion battery systems. This exploration commences with a focused performance assessment of a singular battery system to gauge the efficacy of the platform under scrutiny. Central to this examination are the proportional-integral (PI) controllers, which are adeptly employed to forge cascaded voltage and current control loops. These loops play a pivotal role in the localized converter control intrinsic to the battery system, enabling the swift modulation of both the battery's output voltage and power to align with predefined voltage set-points, as illuminated by the empirical data.

Venturing beyond the solitary battery system, the scope of evaluation broadens to encompass multiple battery systems. This segment of the investigation leverages the SOC balancing control algorithm as delineated in the referenced literature. The experimental apparatus for this phase consists of a platform amalgamating four distinct battery unit types, through which the platform's proficiency in SOC balancing is put to the test. The experimental outcomes affirm the platform's capability in this regard, substantiating its utility and effectiveness.

The forthcoming chapters of this thesis are structured to unfold the layers of development and evaluation that underpin the experimental platform. Chapter 3 is dedicated to elucidating the intricacies of the platform's development. It comprehensively covers the architectural blueprint of the platform, the nuances of converter control mechanisms, the methodologies employed in data collection, and the algorithms underpinning SOC estimation. This chapter aims to provide a holistic overview of the technical and conceptual framework that facilitates the platform's operation.

Subsequently, Chapter 4 presents a detailed account of the experimental tests conducted to scrutinize the platform's operational viability. This chapter is particularly illuminating as it showcases experimental findings pertaining to the control of SOC

balance across multiple battery systems and the regulation of voltage within single battery systems. Through this exposition, the thesis aims to validate the platform's designed functionalities and highlight its potential applications.

Concluding the discourse, Chapter 5 encapsulates the essence of the thesis. It reflects on the journey of development and evaluation that the experimental platform has undergone, summarizing key insights and outcomes. This chapter not only reaffirms the contributions of the platform to the realm of battery management systems but also hints at future avenues for research and enhancement, thereby setting the stage for subsequent explorations in this domain.

# Chapter 2

# Preliminaries

## 2.1 Buck Converter Design

In order to construct a robust battery control system, it is imperative to regulate the output voltage of the battery. To achieve this objective, a buck converter is used. The components are listed in Table 1. The buck converter, a form of non-isolated DC-to-DC switching converter, efficiently reduces higher DC voltages from the supply to lower DC voltages at the load, with efficiencies nearing 90%. This efficiency is significantly superior to that of other DC step-down methods, such as linear regulators. The foundational topology of the buck converter utilized is depicted in Fig. 2.1.

The buck converter incorporates two switches—typically a diode (D1) and a transistor (Q1), an inductor (L1), and a capacitor (C1). The transistor Q1's gate receives a control signal, usually a PWM signal generated by a microcontroller or a dedicated DC switching controller. Activation of Q1 permits current flow from the source, through L1, and into the load, charging the output capacitor C1 in the process. When Q1 is deactivated, the inductor's current continuity forces a voltage adjust-

Table 2.1: Component Specifications

| Name | Product Number | Important Parameters |
|---|---|---|
| D1, D2 | GSGC1545SA | Rectifier, Schottky, 15A, 45V, E |
| Q1 | IRLZ44SPBF | N-Channel 60 V 50A (Tc) 3.7W (Ta), 150W (Tc) |
| L1 | SBC6-4R7-802 | 4.7 µH Unshielded Drum Core |
| C1 | TPSD477M006R0100 | 470 µF Molded Tantalum Capacitors |
| C2 | RL80J102MDN1KX | 1000 µF 6.3 V Aluminum |
| C3 | FK16X7R1C106KR020 | 10 µF ±10% 16V Ceramic Capacitor X7R Radial |
| R1 | WSL2010R1000FEA18 | 100 mOhms ±1% 1W Chip Resistor |

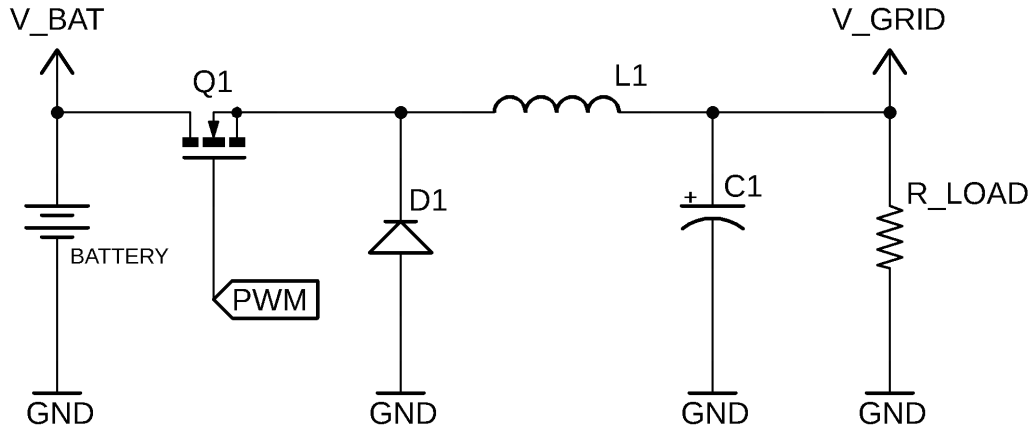


Figure 2.1: Topology of the buck converter.

ment across L1, enabling diode D1 to maintain current flow through the load while C1 discharges. The duty cycle of the PWM signal thus modulates the output voltage, which inherently exhibits some ripple due to the switching nature of the topology. Factors such as the switching frequency, inductor and capacitor values, and circuit parasitics influence the ripple magnitude.

## 2.2 PI Control

Fig. 1.1 illustrates a system diagram with multiple battery cells in operation, currently utilizing a single battery-powered cell to verify the system's capability to control the battery output at a specified voltage.

The battery control system employs a dual-layer PI (Proportional-Integral) control algorithm, a staple in industrial control systems for its feedback loop mechanism. A detailed schematic of the operating system design is presented in Fig. 2.2, providing a comprehensive view of the system architecture, including critical components, interconnections, and signaling pathways. This schematic is essential for understanding the subsystems' interactions within the BMS, highlighting the integration of hardware and software components, data exchange protocols, and the underlying control logic.

This blueprint delineates the PI controller's adaptability in regulating the charging and discharging processes, adjusting currents to mitigate voltage deviations and ensuring balanced cell operation. The BMS's control algorithm leverages a two-tier PI control scheme for effective voltage and current regulation across battery cells in an energy storage unit (ESU).

Consider the control process for battery 1 and its associated buck converter as an example. The initial PI controller, focused on Voltage Control, uses the Target Voltage 1 as its setpoint, modulating the interfacing converter's input to align the output voltage with the target. The output from this PI stage (PI Output 1) acts as a directive for the subsequent control phase—current control.

The following PI controller receives PI Output 1, comparing it against the ESU's actual output current. Adjustments made based on this comparison (PI Output 2) aim to achieve the target voltage with increased accuracy. This layered PI approach

ensures precise power output control from the ESU, with the second PI controller generating a control signal (PWM) to manage buck converter 1, thus achieving the target voltage. The explored control algorithm adopts a cascaded method, utilizing two layers of PI controllers to maintain the system's current within desired parameters, facilitating regulation through nested layers of control to maintain adherence to the specified target current.

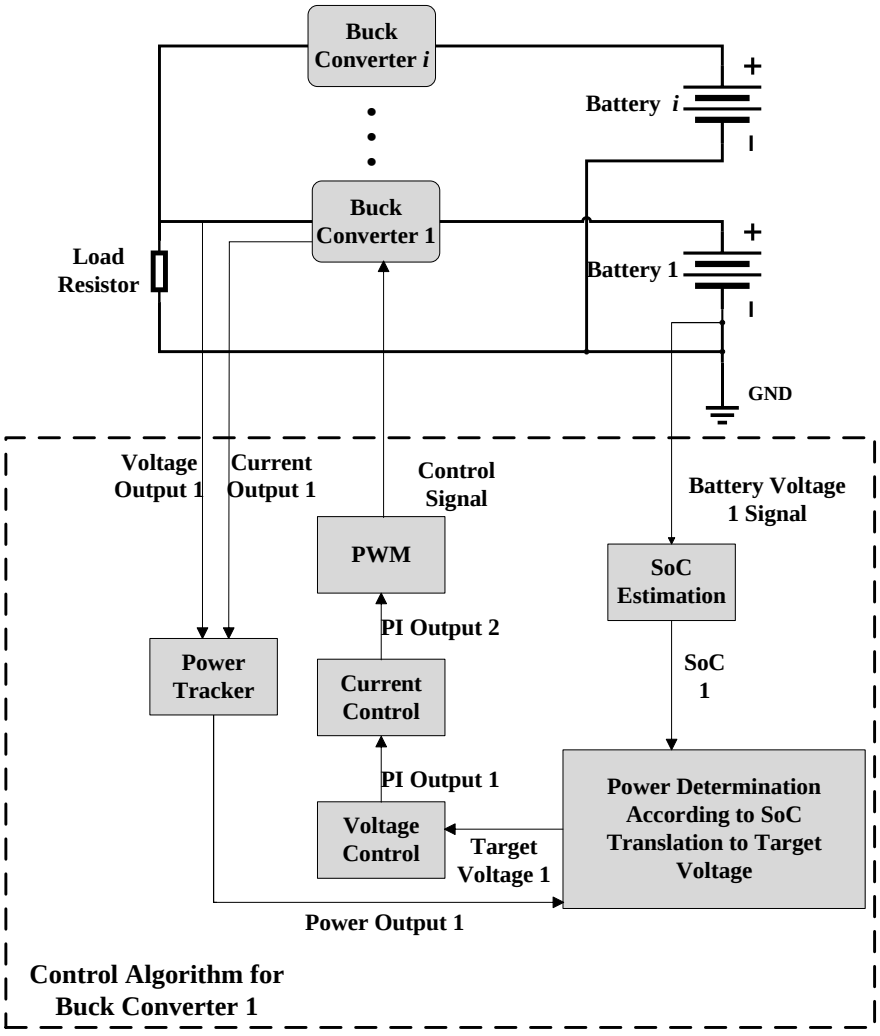


Figure 2.2: Schematic of the local control for a buck converter.

# Chapter 3

# Development of the Platform

As seen in Fig. 1.1, we demonstrate in this chapter the creation of an experimental platform for lithium-ion battery systems.

## 3.1 Platform Architecture

The TMS320F28335 is the cornerstone of the experimental platform designed to manage the battery's charging and discharging processes. The TMS320C2000 series DSPs are notable for their hybrid functionality, merging the benefits of high-performance digital signal processors with microcontrollers to enable robust control and signal processing capabilities. These DSPs feature an integration of Flash memory, a rapid AD converter, an enhanced CAN module, an event manager, a quadrature encoding circuit interface, and peripherals such as a multi-channel buffered serial port, facilitating the development of high-performance digital control systems at a reduced cost.

At the heart of the experimental platform is the DSP chip TMS320F28335, chosen for its accurate regulation of EPWM output values and sophisticated signal processing capabilities, which are crucial for implementing complex control algorithms.

Figure 3.1 showcases a prototype of the developed experimental platform.

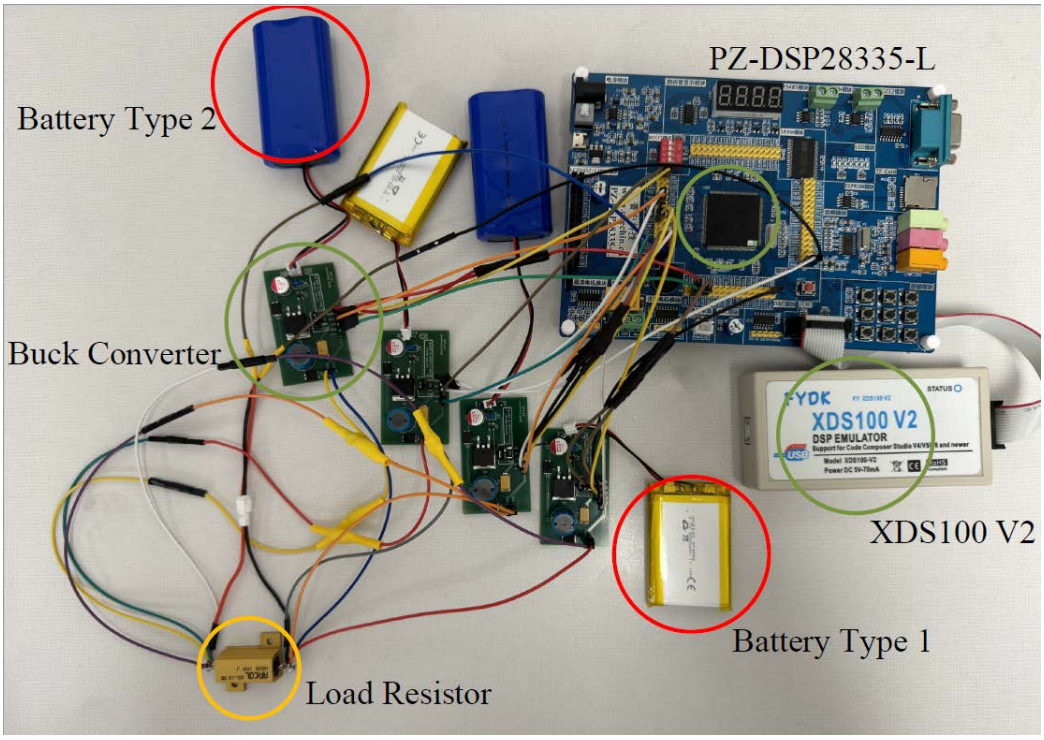


Figure 3.1: Prototype of the experimental platform.

The hardware foundation is provided by the PZ-DSP28335-L development board, incorporating the TMS320F28335 DSP chip. This board is equipped with multiple ADC interfaces for real-time voltage monitoring—essential for the control algorithm—and an RS232 module for data communication with a host computer. For comprehensive testing and debugging, the XDS 100V2 emulator is employed. A constant resistor load of 1.6 Ohms ensures a stable testing environment for the Battery Management System (BMS), under uniform load conditions. The experimental setup includes two types of battery packs: 974058 rechargeable lithium-ion polymer batteries (Battery Type 1, 3.7V, 3000mAh) and 18650 rechargeable lithium-ion batteries (Battery Type 2, 3.7V, 4400mAh), each interfaced with a buck converter to maintain consistency across battery packs.

A DC-DC buck converter is utilized to effectively control the output voltage of the

battery system. Table 1 lists the components of the designed buck converter. This non-isolated DC-DC switching converter efficiently lowers a higher input voltage to a desired lower output voltage, with its basic topology depicted in Fig. 2.1.

To facilitate parallel operations of multiple buck converters, enhancements to the base schematic depicted in Fig. 2.1 were necessary, as shown in Fig. 3.2. Modifications include the addition of a diode (D2) for current OR-ing, a gate driver (U1) for optimized MOSFET performance, and a current-sensing resistor (R1) for precise supply current measurement. Further augmentations such as a battery connector (JP2), test points (JP4, JP5), and a swappable load resistance (JP6) enhance testing flexibility. Stability and control improvements are achieved through the inclusion of an input capacitor (C2) and an external microcontroller connection header (JP3).

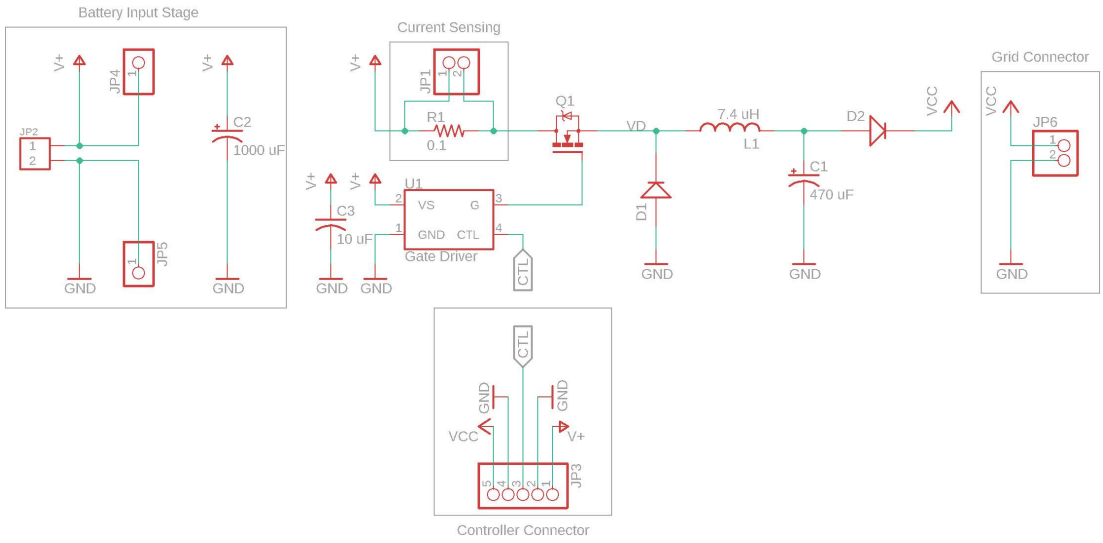


Figure 3.2: Schematic of the enhanced buck converter.

The adapted schematic is illustrated in Fig. 3.2, which has been transformed into a board layout for manufacturing, as demonstrated in Fig. 3.3. The PCB layout employs a color scheme indicative of its layers and elements: red and blue for the top and bottom copper layers, respectively, green for through-hole drills, and white for silkscreen elements, with dimensions of 56x33mm. Fig. 3.4 presents a render of

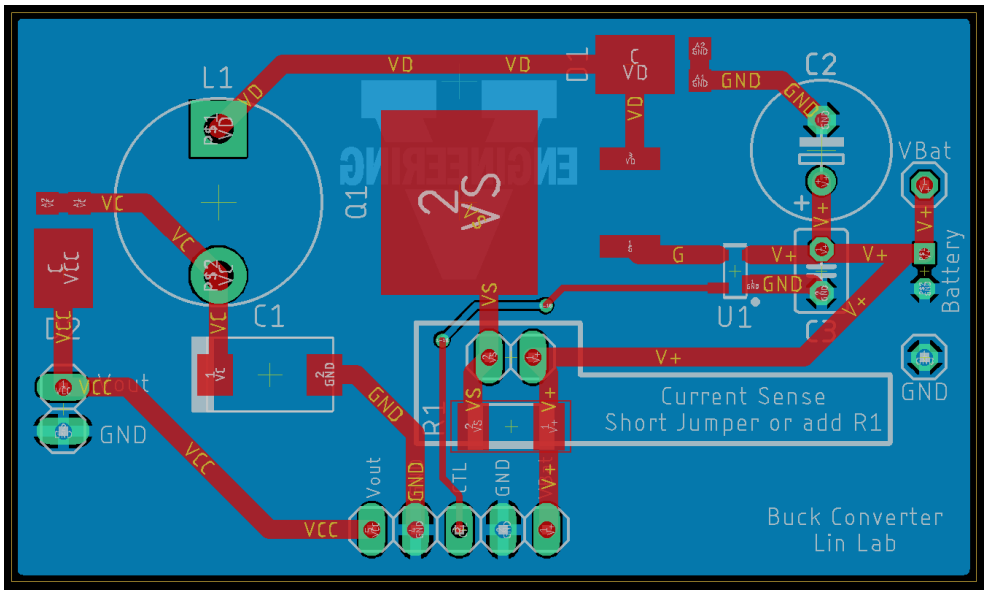


Figure 3.3: PCB layout for fabrication.

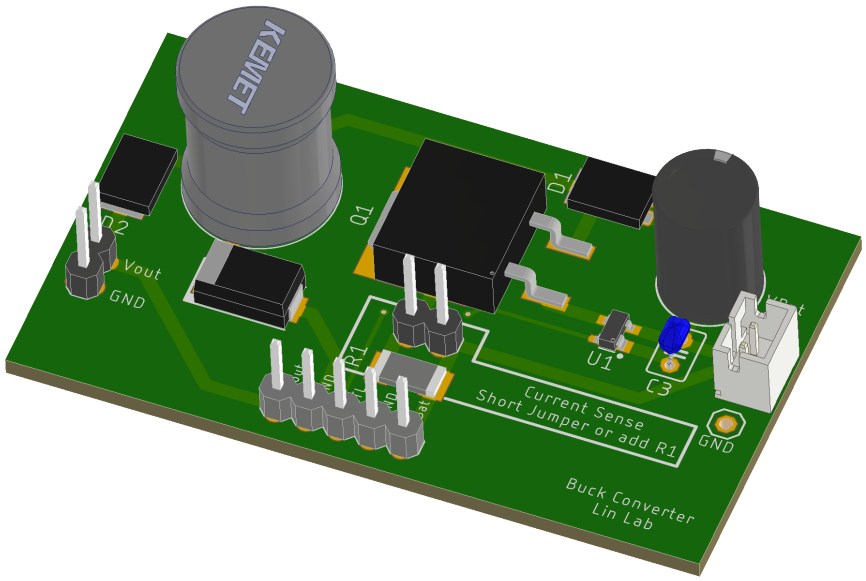


Figure 3.4: Schematic of the PCB.

the PCB with components mounted, employing a 4-layer FR4-TG 150-160 substrate, 1oz copper plating, and HASL finishing. Surface-mount components are affixed via stenciling and reflow soldering, while through-hole components are soldered manually. The completed PCB post-fabrication is showcased in Fig. 3.5.

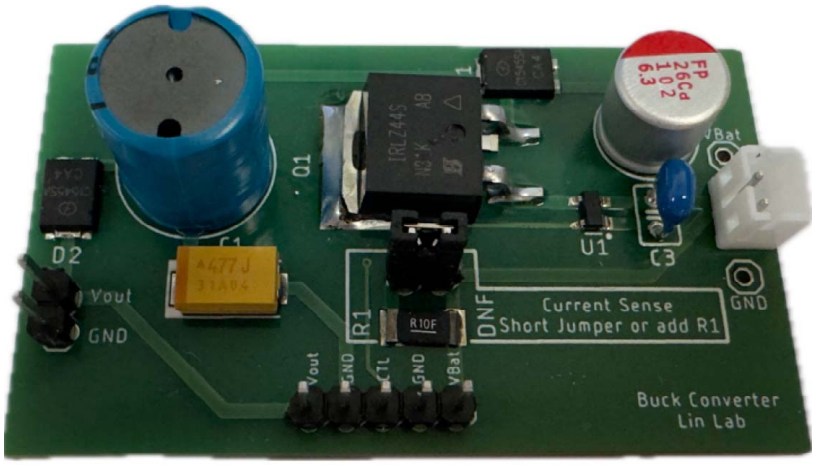


Figure 3.5: Prototype of the enhanced buck converter.

## 3.2 Converter Control

A schematic of the local control for a buck converter within a battery system is depicted in Fig. 2.2, employing two cascaded Proportional-Integral (PI) controllers to regulate the output voltage and current of the converter. To elucidate the control process, consider the buck converter associated with battery 1. The voltage controller (PI controller) receives as its input the deviation between the reference voltage, defined as Target Voltage 1, and the actual output voltage of converter 1. This reference voltage corresponds to the power set-point determined by the power control algorithm for State of Charge (SOC) balancing. The output from the voltage controller, referred to as PI Output 1, serves as the reference current for the current controller. For the current controller (another PI controller), the input is the difference between this reference current and the measured output current of converter 1. The current controller's output, termed PI Output 2, is then utilized to generate a Pulse Width Modulation (PWM) signal, acting as the control signal for the switch of converter

1. Through these cascaded PI controllers, the output power of converter 1 is able to swiftly align with the desired power set-point.

The power set-point for the converter's output power is ascertained by SOC balancing control algorithms. In this study, the control algorithm delineated in [46] is implemented as follows. For each battery unit $i$, we define:

$$\tau_i = SOC_i \times Q_i \times V_{\text{in}i} \tag{3.1}$$

where $SOC_i$ represents the SOC, $Q_i$ the battery's capacity, and $V_{\text{in}i}$ the battery's voltage, which also corresponds to the input voltage for buck converter $i$. Consequently, the power set-point for buck converter $i$ is given by:

$$P_{\text{ref}i} = \left(\frac{\tau_i}{\tau_{\text{avg}}}\right) \times \frac{P_{\text{load}}}{N} \tag{3.2}$$

where $\tau_{\text{avg}} = \frac{1}{N}\sum_{i=1}^{N} \tau_i$, with $N$ denoting the number of battery units, and $P_{\text{load}}$ the load power.

## 3.3 Data Collection

Given the PZ-DSP28335-L development board's integration of multiple ADC (Analog-to-Digital Converter) jumpers, it is feasible to sequentially measure the voltage at these jumpers. The ADC-converted digital values are used to determine the interface voltage value, according to the equation:

$$\text{Voltage Value} = \frac{3 \times \text{ADC Data Value}}{4096} \tag{3.3}$$

In a system powered by a single battery, the output power can be directly calculated from the measured output voltage. With a constant resistive load, the relationship between the output power $P_{\text{output}}$ and the load power $P_{\text{load}}$ is expressed as:

$$P_{\text{load}} = \frac{V_{\text{out}}^2}{R_{\text{load}}} \tag{3.4}$$

Given that the load is a constant resistor, the output current is derived from the buck converter's output voltage as:

$$I_{\text{out}} = \frac{V_{\text{out}}}{R_{\text{load}}} \tag{3.5}$$

Furthermore, the battery's output power is defined by:

$$P_{\text{out}} = V_{\text{out}} \times I_{\text{load}} = \frac{V_{\text{out}}^2}{R_{\text{load}}} \tag{3.6}$$

However, for configurations where multiple battery units are connected in parallel, direct calculation of branch circuit current as in a single battery setup is not straightforward. To circumvent this, a measuring resistor is introduced in each branch post the buck converter, as illustrated in Fig. 3.6, enabling branch current measurement. The resistance of the measuring resistor is set at $R_{\text{MeasureResistor}} = 0.3\Omega$. The voltage

drop across measuring resistor 1, upon measuring the output voltage $V_{\text{out1}}$ of converter 1, is calculated by:

$$V_{\text{MeasureResistor1}} = V_{\text{load}} - V_{\text{out1}} \tag{3.7}$$

where $V_{\text{load}}$ denotes the voltage measured across the load. The output current for buck converter 1 in the branch equals the current through measure resistor 1, determined as:

$$I_{\text{out1}} = \frac{V_{\text{measure1}}}{R_{\text{MeasureResistor}}} \tag{3.8}$$

Consequently, the output power of buck converter 1 is given by:

$$P_{\text{out1}} = V_{\text{out1}} \times I_{\text{out1}} \tag{3.9}$$

The output power $P_{\text{out1}}$ in (3.9) represents the measured output power for buck converter 1. The control aim is to ensure this measured output power $P_{\text{out1}}$ follows the power set-point $P_{\text{ref}i}$ as specified by (3.2).

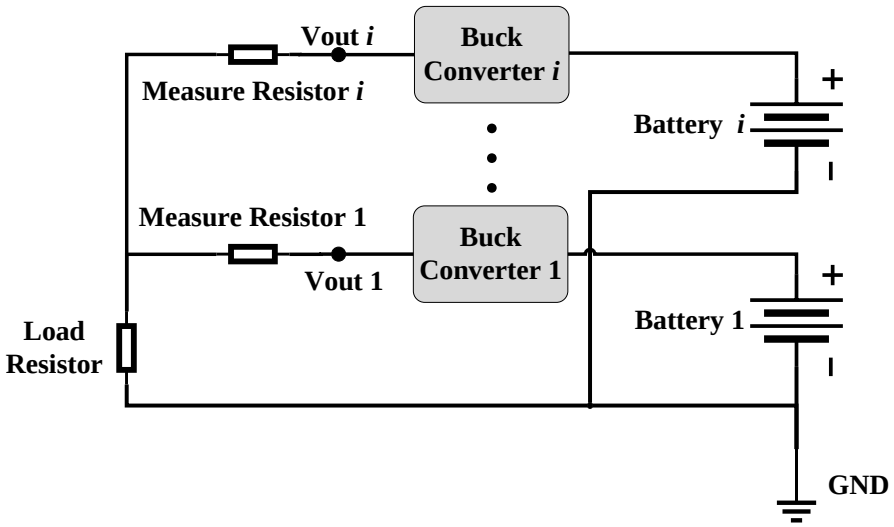


Figure 3.6: Schematic of multiple battery units in parallel.

## 3.4 SOC Estimation

This study employs a look-up table methodology for estimating the SOC of the battery, utilizing real-time voltage readings during battery operation. A pre-established table correlating SOC values to battery voltage enables the immediate determination of SOC upon acquiring the battery's voltage. The process involved in constructing the SOC-voltage relationship table is explained in depth, highlighting the practicality and accuracy of this approach for real-time SOC estimation.

The Equivalent Series Resistance (ESR) of a battery, a critical parameter affecting its performance and efficiency, is quantified through a method beginning with the open-circuit voltage (OCV) measurement. The procedure initiates with measuring the OCV, denoted as $U_0$, followed by momentarily short-circuiting the battery terminals to establish a baseline voltage. Subsequently, a resistor, $R_0$, is connected in parallel to the terminals to initiate a discharge cycle. The voltage, $U$, across the battery terminals is monitored during this phase.

The ESR is computed utilizing the equation:

$$\text{ESR} = \frac{U_0 - U}{U/R_0} \tag{3.10}$$

Applying this methodology to two different lithium battery types yielded:

- For Battery Type 1 (3000 mAh, 3.7V), an ESR of 0.142 ohm was calculated.
- For Battery Type 2 (4400 mAh, 3.7V), the ESR was found to be 0.202 ohm.

These measurements afford insights into the electrical characteristics of the batteries, facilitating a comparative analysis of their performance predicated on internal resistance metrics.

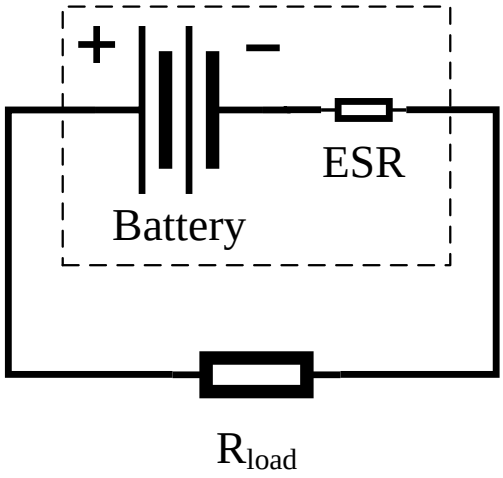


Figure 3.7: Schematic diagram of measurement circuit.

Fig. 3.7 illustrates the circuit configuration employed for measuring the correlation between battery voltage and State of Charge (SOC). An external load resistor, characterized by a resistance $R_{\text{load}}$, is connected to the battery.

The battery discharges continuously from a fully charged state, maintaining a constant discharge rate. The closed-loop current, $I_{\text{closed\_loop}}$, is defined as:

$$I_{\text{closed\_loop}} = \frac{V_{\text{load}}}{R_{\text{load}}} \tag{3.11}$$

where $I_{\text{closed\_loop}}$ represents the operating current of the circuit, and $V_{\text{load}}$ denotes the voltage across the load resistor.

Utilizing the previously calculated equivalent series resistance (ESR), the voltage drop across the battery's internal resistance, $V_{\text{ESR}}$, is estimated by:

$$V_{\text{ESR}} = I_{\text{closed\_loop}} \times \text{ESR} \tag{3.12}$$

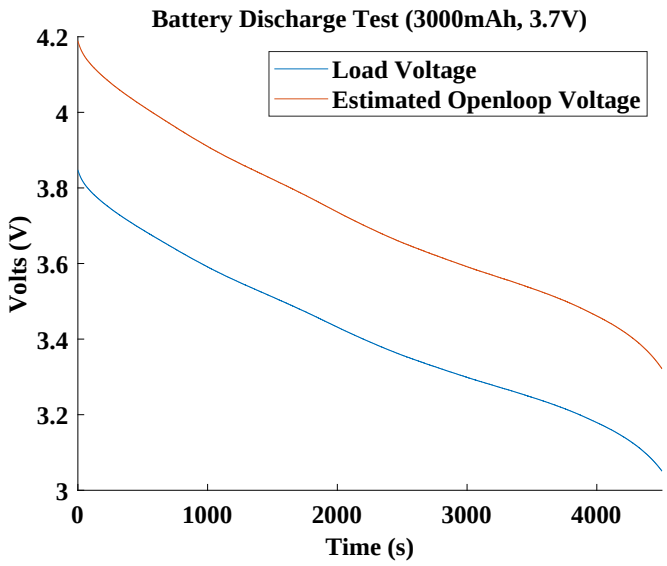


Figure 3.8: Relationship between open-loop and operating voltage (3000mAh).

Consequently, the open-circuit voltage, $V_{\text{open\_loop}}$, can be expressed as:

$$V_{\text{open\_loop}} = V_{\text{load}} + V_{\text{ESR}} \tag{3.13}$$

Taking Battery Type 1 (3000mAh, 3.7V) as an instance, Fig. 3.8 delineates the relationship between the open-circuit voltage and the operating voltage under load conditions. The power consumed by the load, $P_{\text{load}}$, is calculated as:

$$P_{\text{load}} = \frac{V_{\text{load}}^2}{R_{\text{load}}} \tag{3.14}$$

The total energy expended by the battery throughout the discharge process, $E_{\text{consumed}}$, is obtained through the integration of $P_{\text{load}}$ over time. The total energy expended by the battery throughout the discharge process, $E_{\text{consumed}}$, is obtained

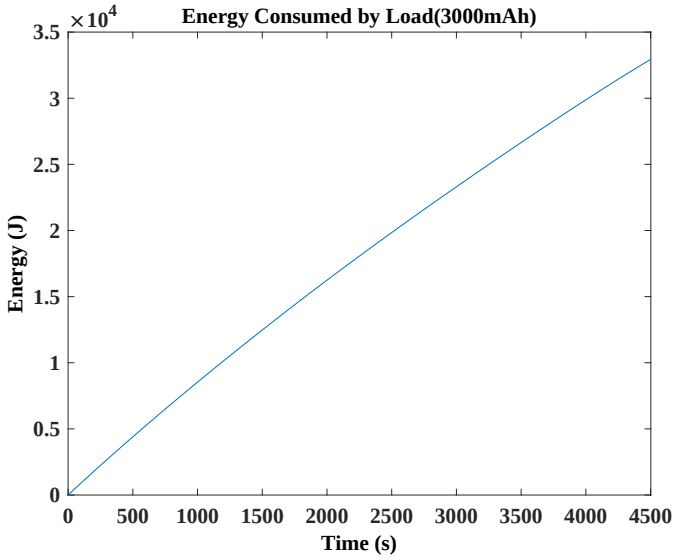


Figure 3.9: Energy consumed by load (3000mAh).

through the integration of $P_{\text{load}}$ over time:

$$E_{\text{consumed}} = \int P_{\text{load}} \, \mathrm{d}t \tag{3.15}$$

Fig. 3.9 exhibits the energy consumption over time. The consumed charge, $C_{\text{consumed}}$, is derived from the energy through the equation:

$$C_{\text{consumed}} = \frac{E_{\text{consumed}}}{V_{\text{load}} \times 3.6} \tag{3.16}$$

Fig. 3.10 presents the continuous power consumption during the experiment. By comparing this with the initial battery charge $C_0 = 3300\text{mAh}$, the SOC can be determined as follows:

$$\text{SOC} = \left( \frac{C_0 - C_{\text{consumed}}}{C_0} \right) \times 100\% \tag{3.17}$$

As illustrated in Fig. 3.11, in conjunction with the voltage-time relationship shown

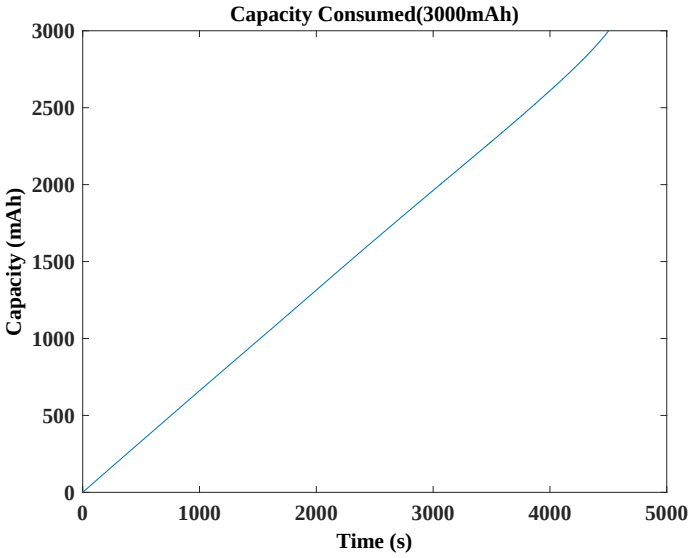


Figure 3.10: Capacity consumed (3000mAh).

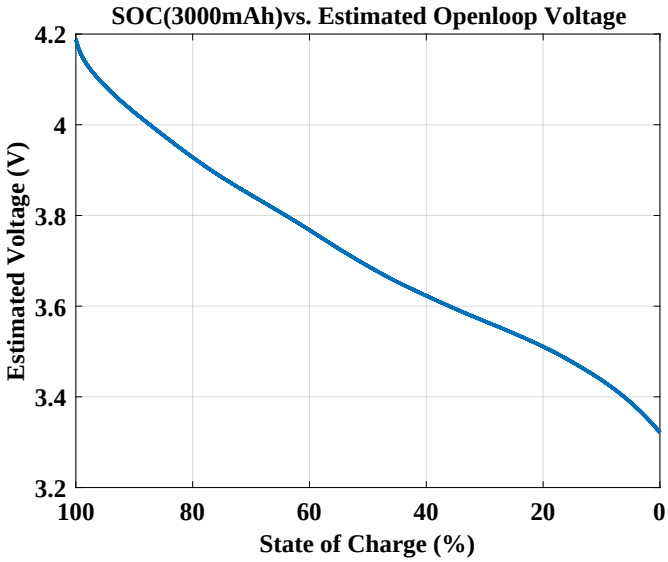


Figure 3.11: SOC versus open-loop voltage (3000mAh).

in Fig. 3.8, a plot of SOC versus voltage is derived. This methodology enables the determination of the battery's SOC at any given moment during the circuit experiment by measuring the battery voltage, crucial for the accurate estimation of the battery's state.

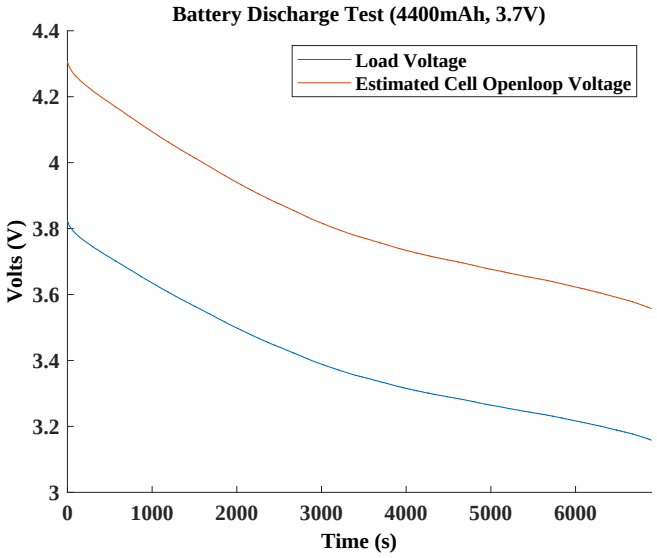


Figure 3.12: Relationship between open-loop and operating voltage (4400mAh).

Similarly, for Battery Type 2 (4400mAh, 3.7V), Fig. 3.12 and Fig. 3.13 demonstrate the open-circuit and operating voltage relationship, alongside its SOC versus open-circuit voltage curve, respectively. In the subsequent battery control experiment, the State of Charge (SOC) of the battery is ascertainable by reading the voltage across the battery. This voltage measurement is then incorporated into the battery control algorithm.

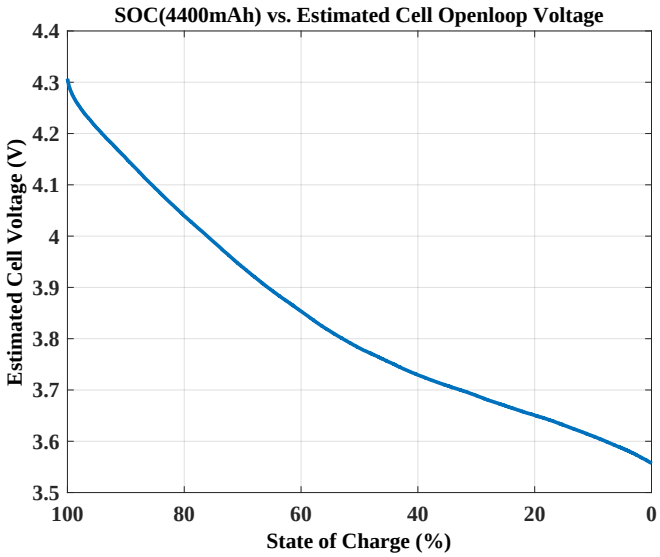


Figure 3.13: SOC versus open-loop voltage (4400mAh).

# Chapter 4

# Evaluation of the Platform

## 4.1 Performance Evaluation for Single Battery Systems

We start by analyzing the performance of a single battery system. We must choose the right parameters for two PI controllers in the experimental test. Each PI controller is initialized with a set of gains tailored to the system's response characteristics. Within the scope of the test conditions formulated for this study, two distinct sets of PI control parameters were meticulously assessed. Specifically, the first controller is configured with $P = 12$, $I = 1$, which implies that the derivative component is not active in the control process. This tuning implies that the control strategy prioritizes the steady-state error correction and the system's responsiveness without the derivative action's influence. The operation of the controller is a cyclical process of error computation, where the difference between the expected and the actual current values dictates the control action. The PI output is a cumulative sum of the proportional and the integrated terms, adjusted at each cycle to steer the system toward the target current.

Following the initial voltage adjustment, a second PI controller receives the processed signal for further refinement. The second PI controller, with a finer tuning resolution, is initialized with $P_1 = 0.1$, $I_1 = 0.05$ . This controller employs a similar error computation mechanism but operates with different gain settings, signifying its role in fine-tuning the control signal to match the exact target current values. This secondary PI controller fine-tunes the adjustments made by the first controller, thereby achieving a highly accurate current output.

The algorithmic structure ensures that the first PI controller's output is meticulously adjusted by the second, enabling a higher fidelity in current regulation. The subsequent control loop, sensitive to the variations in current, acts on these deviations to perfect the control signal. The collective operation of the dual PI controllers ensures a robust control mechanism. The first controller makes coarse adjustments, while the second refines them, addressing complexities and non-linearities within the system. Continuity in the control process is maintained by storing the last error values, which reflects a system's past behavior to inform subsequent control actions.

To evaluate the dynamic performance of the designed battery control system, a step response test was conducted. The experimental setup included the connection of a solitary battery cell, with the Load consisting of a solid-state resistor. Establishing and attaining a specific target voltage value under these conditions served as a confirmation of the system's power tracking capabilities. This is due to the direct relationship between the output power, $P_{\text{output}}$, and the load power, $P_{\text{load}}$, which, in the presence of a constant resistance, can be expressed as

$$P_{\text{load}} = \frac{V_{\text{out}}^2}{R_{\text{load}}} \tag{4.1}$$

The successful attainment of the target voltage not only underscores the precision of

the control system but also its efficiency in power regulation. Given that the output power is a function of the square of the output voltage over the load resistance, reaching the target voltage is synonymous with achieving the desired power output. This aspect of the experiment illustrates the system's proficiency in maintaining the energy flow at predetermined levels.This experiment is critical for assessing the system's responsiveness to changes in control input and its ability to track varying voltage setpoints over time. The test involved applying a discrete step function to the voltage setpoint of an individual battery cell within the system. The step function consisted of a sequence of voltage levels.

The target voltage as a function of time, targetvoltage($t$), for a repeating 40-second cycle is defined by the following piecewise function with non-negative integer $i$ denoting the cycle index:

$$\text{targetvoltage}(t) = \begin{cases} 0.5V & \text{if } 40i \leq t < 40i + 10 \\ 1.0V & \text{if } 40i + 10 \leq t < 40i + 20 \\ 1.5V & \text{if } 40i + 20 \leq t < 40i + 30 \\ 2.0V & \text{if } 40i + 30 \leq t < 40(i + 1) \end{cases} \tag{4.2}$$

where $i$ a nonnegative integer.

The response of the battery cell to the step function was recorded and is depicted in Fig. 4.1. The results demonstrate the system's capability to accurately track the step changes in the voltage setpoint. The transition between voltage levels illustrates the control system's precision and stability, confirming its compliance with the predefined control specifications. Each step increase in the setpoint voltage was followed by a corresponding and timely adjustment in the battery cell's output, showcasing the efficacy of the PI control algorithm in maintaining the desired voltage levels. The

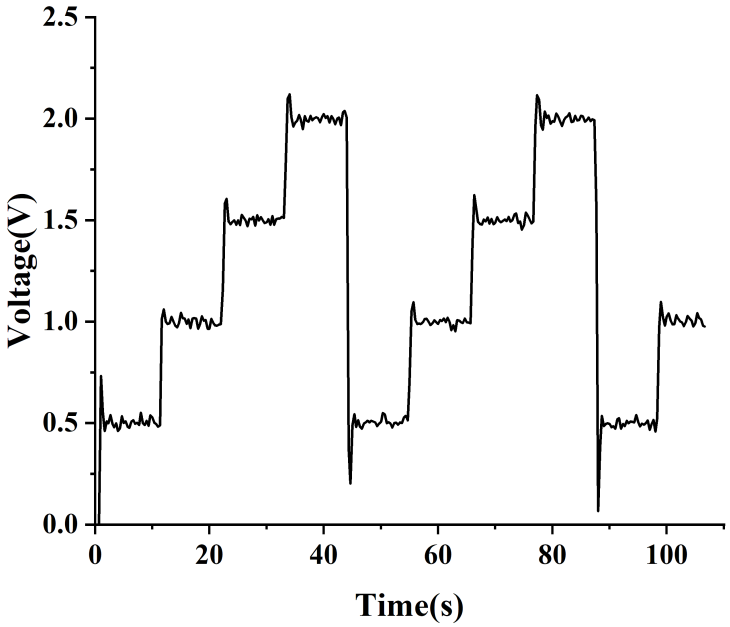


Figure 4.1: Experimental result for voltage regulation of a single battery system.

system's performance in this experiment substantiates its potential applicability in real-world scenarios, where precise voltage control is imperative.

## 4.2 Performance Evaluation for Multiple Battery Systems

The actual output value of the Buck converter will be utilized as the actual value in the PI algorithm, aiding the platform in controlling the battery output. In [46], the total voltage supplied to the load in the case of $N$ power supply units is:

$$P_{\text{load}} = \sum_{i=1}^{N} P_i \tag{4.3}$$

where $P_i$ is the output power of the $i^{th}$ buck converter. A coefficient $\tau_i$ for the $i^{th}$ battery cell is defined as:

$$\tau_i = SOC_i \times Q_i \times V_{\text{out}i} \tag{4.4}$$

Here, $SOC_i$ is the state of charge value of the battery, $Q_i$ is the capacity of the battery, and $V_{\text{out}i}$ is the output voltage after passing through the buck converter. The average value of $\tau$ is computed as:

$$\tau_{\text{avg}} = \frac{1}{N} \sum_{i=1}^{N} \tau_i \tag{4.5}$$

The target output value of Buck Converter $i$ is then:

$$P_i = \left( \frac{\tau_i}{\tau_{\text{avg}}} \right) \times \frac{P_{\text{load}}}{N} \tag{4.6}$$

Setting $P_{\text{load}} = 5W$ connects to the platform system. Fig. 3.1 presents the actual results after connecting four battery-powered units; two Battery Type 1 and two Battery Type 2 are utilized.

Fig. 4.2 presents the outcomes of the experimental tests conducted to assess the

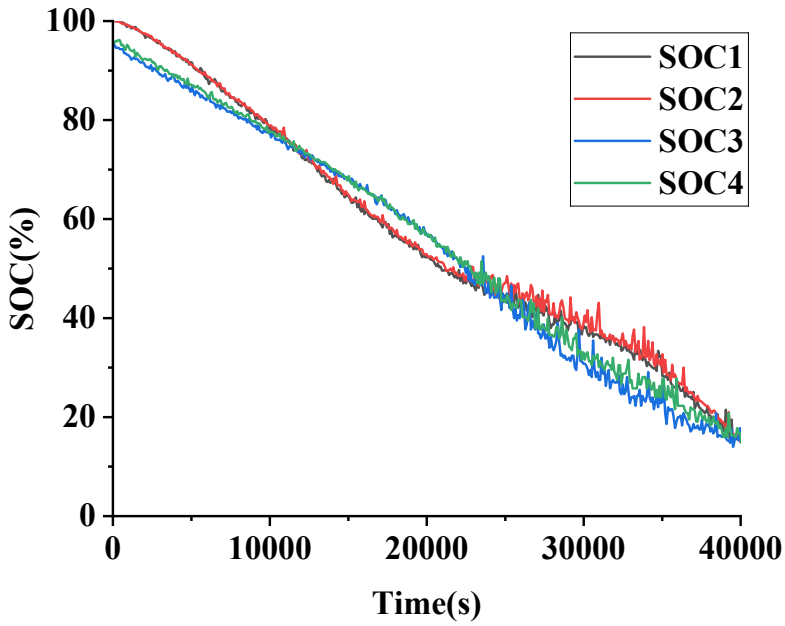


Figure 4.2: Experimental result for SOC balancing among four battery systems.

SOC balancing capabilities of the proposed battery management system. The tests involved two sets of batteries, designated as SOC1 and SOC2 for Battery Type 1, and SOC3 and SOC4 for Battery Type 2. It was observed that despite starting from different SOC levels, batteries of varying specifications converged to a similar SOC value, achieving equilibrium at approximately 20%. However, fluctuations in the measured voltage values were noted, attributable to the system's measurement accuracy. This, in turn, led to observable variations in the recorded data.

Fig. 4.3 presents the result of the experimental test conducted to assess the SOC balancing capabilities by applying the control algorithm (3.2). In Fig. 4.3, SOC 1 is for Type 1 batteries, and SOC 2 and SOC 3 are for Type 2 batteries. It can be observed that the SOC levels converge towards the same value but with some fluctuations. This is because of inaccuracy in the measurement of the voltage values.

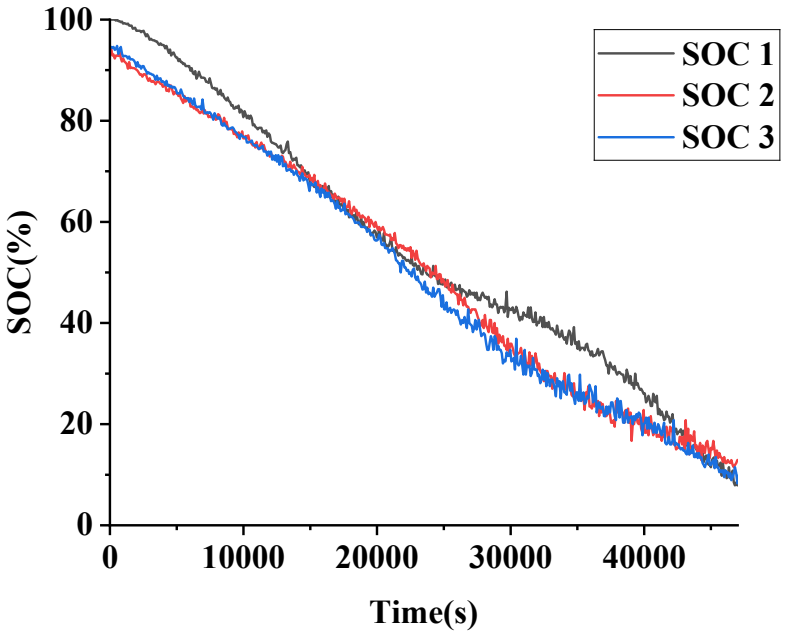


Figure 4.3: Experimental result for SOC balancing among three battery systems.

# Chapter 5

# Conclusions and Future Works

## 5.1 Conclusions

This thesis has introduced and evaluated an experimental platform designed for the testing and validation of Battery Management System (BMS) algorithms aimed at achieving State-of-Charge (SOC) balancing in lithium-ion battery systems. The platform, developed around a DSP chip (TMS320F28335), custom-designed buck converter, various battery packs, and load resistors, offers a versatile environment for adjusting parameters and testing different BMS algorithms. Through the application of a selected BMS algorithm, we demonstrated the platform's capability in managing SOC balancing among heterogeneous battery units, showcasing its effectiveness and validating its design choices.

The experimental results provide compelling evidence of the platform's utility in both single and multiple battery system configurations. For single battery systems, the implementation of cascaded PI controllers allowed for precise control of the battery's output, quickly aligning it with set voltage points. In the context of multiple battery systems, our experiments confirmed the platform's proficiency in maintaining

SOC balancing across battery units, despite the presence of measurement inaccuracies and fluctuations. These findings underscore the potential of our experimental platform to serve as a valuable tool in the research and development of advanced BMS algorithms.

The successful development and evaluation of the experimental platform mark a significant step forward in the study of SOC balancing control strategies for lithium-ion battery systems. By facilitating a deeper understanding and testing of various BMS algorithms, the platform aids in the advancement of battery technology, contributing to more efficient and reliable battery energy storage solutions. Furthermore, the platform's design enables researchers to simulate real-world conditions, offering insights into the performance and potential challenges of implementing BMS algorithms in practical applications.

## 5.2 Future Works

Looking ahead, several avenues for future research emerge from this study. Firstly, there is a need to explore and implement distributed SOC balancing control algorithms to test more complex scenarios that closely mimic real-world battery system configurations. Such studies could enhance our understanding of the dynamics involved in managing SOC across battery units interconnected in large-scale battery systems. Secondly, efforts will be directed toward refining the buck converter's structure. This would simplify the process of measuring voltage and current directly from the battery, thereby reducing complexity and potential sources of error in experiments. Finally, enhancing the accuracy of measurements stands as a critical objective. Improved precision in SOC estimation and other relevant metrics is crucial for the effective assessment and optimization of BMS algorithms. Addressing these

challenges will pave the way for the development of more sophisticated and efficient battery management solutions, contributing to the broader adoption of renewable energy sources and the advancement of sustainable energy storage technologies.

# Bibliography

[1] F. R. McLarnon and E. J. Cairns, "Energy storage," *Annual Review of Energy*, vol. 14, no. 1, pp. 241–271, 1989.

[2] J. N. Baker and A. Collinson, "Electrical energy storage at the turn of the millennium," *Power Engineering Journal*, vol. 13, no. 3, pp. 107–112, 1999.

[3] M. Y. Suberu, M. W. Mustafa, and N. Bashir, "Energy storage systems for renewable energy power sector integration and mitigation of intermittency," *Renewable and Sustainable Energy Reviews*, vol. 35, pp. 499–514, 2014.

[4] M. C. Kintner-Meyer, P. J. Balducci, C. Jin, T. B. Nguyen, M. A. Elizondo, V. V. Viswanathan, X. Guo, and F. K. Tuffner, "Energy storage for power systems applications: A regional assessment for the northwest power pool (nwpp)," Pacific Northwest National Lab.(PNNL), Tech. Rep. PNNL-19300, 2010.

[5] A. Aktas, K. Erhan, S. Ozdemir, and E. Ozdemir, "Experimental investigation of a new smart energy management algorithm for a hybrid energy storage system in smart grid applications," *Electric Power Systems Research*, vol. 144, pp. 185–196, 2017.

[6] A. Tuohy and M. O'Malley, "Pumped storage in systems with very high wind penetration," *Energy Policy*, vol. 39, no. 4, pp. 1965–1974, 2011.

[7] M. Black and G. Strbac, "Value of bulk energy storage for managing wind power fluctuations," *IEEE Transactions on Energy Conversion*, vol. 22, no. 1, pp. 197–205, 2007.

[8] D. Pudjianto, M. Aunedi, P. Djapic, and G. Strbac, "Whole-systems assessment of the value of energy storage in low-carbon electricity systems," *IEEE Transactions on Smart Grid*, vol. 5, no. 2, pp. 1098–1109, 2013.

[9] H. Chen *et al.*, "Progress in electrical energy storage system: A critical review," *Progress in Natural Science*, vol. 19, no. 3, pp. 291–312, 2009.

[10] F. Duffner, M. Wentker, M. Greenwood, and J. Leker, "Battery cost modeling: A review and directions for future research," *Renewable and Sustainable Energy Reviews*, vol. 127, p. 109872, 2020.

[11] B. M. Gundogdu, S. Nejad, D. T. Gladwin, M. P. Foster, and D. A. Stone, "A battery energy management strategy for UK enhanced frequency response and triad avoidance," *IEEE Transactions on Industrial Electronics*, vol. 65, no. 12, pp. 9509–9517, 2018.

[12] H. Chen, T. N. Cong, W. Yang, C. Tan, Y. Li, and Y. Ding, "Progress in electrical energy storage system: A critical review," *Progress in Natural Science*, vol. 19, no. 3, pp. 291–312, 2009.

[13] J. Kondoh, I. Ishii, H. Yamaguchi *et al.*, "Electrical energy storage systems for energy networks," *Energy Conversion and Management*, vol. 41, no. 17, pp. 1863–1874, 2000.

[14] A. Z. A. L. Shaqsi, K. Sopian, and A. Al-Hinai, "Review of energy storage services, applications, limitations, and benefits," *Energy Reports*, vol. 6, pp. 288–306, 2020.

[15] H. Daneshi and A. K. Srivastava, "Impact of battery energy storage on power system with high wind penetration," in *PES T&D 2012*, 2012, pp. 1–8.

[16] B. Lu and M. Shahidehpour, "Short-term scheduling of battery in a grid-connected pv/battery system," *IEEE Transactions on Power Systems*, vol. 20, no. 2, pp. 1053–1061, 2005.

[17] T. Logenthiran and D. Srinivasan, "Short term generation scheduling of a microgrid," in *TENCON 2009-2009 IEEE Region 10 Conference*, 2009, pp. 1–6.

[18] S. X. Chen, H. B. Gooi, and M. Q. Wang, "Sizing of energy storage for microgrids," *IEEE Transactions on Smart Grid*, vol. 3, no. 1, pp. 142–151, 2011.

[19] I. B. Espedal, A. Jinasena, O. S. Burheim, and J. J. Lamb, "Current trends for state-of-charge (SoC) estimation in lithium-ion battery electric vehicles," *Energies*, vol. 14, no. 11, p. 3284, 2021.

[20] X. Feng, M. Ouyang, X. Liu, L. Lu, Y. Xia, and X. He, "Thermal runaway mechanism of lithium ion battery for electric vehicles: A review," *Energy Storage Materials*, vol. 10, pp. 246–267, 2018.

[21] L. J. Aaldering, J. Leker, and C. H. Song, "Analysis of technological knowledge stock and prediction of its future development potential: The case of lithium-ion batteries," *Journal of Cleaner Production*, vol. 223, pp. 301–311, 2019.

[22] B. Diouf and R. Pode, "Potential of lithium-ion batteries in renewable energy," *Renewable Energy*, vol. 76, pp. 375–380, 2015.

[23] M. S. Whittingham, "Lithium batteries and cathode materials," *Chemical Reviews*, vol. 104, no. 10, pp. 4271–4302, 2004.

[24] T. Kim, W. Song, D. Y. Son, L. K. Ono, and Y. Qi, "Lithium-ion batteries: outlook on present, future, and hybridized technologies," *Journal of Materials Chemistry A*, vol. 7, no. 7, pp. 2942–2964, 2019.

[25] G. E. Blomgren, "The development and future of lithium ion batteries," *Journal of The Electrochemical Society*, vol. 164, no. 1, p. A5019, 2016.

[26] M. Li, J. Lu, Z. Chen *et al.*, "30 years of lithium-ion batteries," *Advanced Materials*, vol. 30, no. 33, p. 1800561, 2018.

[27] J. R. Dahn, T. Zheng, Y. Liu, and J. S. Xue, "Mechanisms for lithium insertion in carbonaceous materials," *Science*, vol. 270, no. 5236, pp. 590–593, 1995.

[28] G. Pistoia, *Lithium-ion batteries: advances and applications*. Newnes, 2013.

[29] L. Xie, C. Tang, Z. Bi, M. Song, Y. Fan, C. Yan, X. Li, F. Su, Q. Zhang, and C. Chen, "Hard carbon anodes for next-generation li-ion batteries: review and perspective," *Advanced Energy Materials*, vol. 11, no. 38, p. 2101650, 2021.

[30] B. Scrosati, J. Hassoun, and Y.-K. Sun, "Lithium-ion batteries. a look into the future," *Energy & Environmental Science*, vol. 4, no. 9, pp. 3287–3295, 2011.

[31] M. Yoshio, R. J. Brodd, and A. Kozawa, *Lithium-ion batteries*. Springer, 2009, vol. 1.

[32] Z. Lu, D. D. MacNeil, and J. R. Dahn, "Layered cathode materials $li[ni_x li_{(1/3-2x/3)} mn_{(2/3-x)}]o_2$ for lithium-ion batteries," *Electrochemical and Solid-State Letters*, vol. 4, no. 11, p. A191, 2001.

[33] M. Li, Z. Chen, K. Amine, and J. Lu, *Nickel-based Cathode for Li-ion Batteries*. CRC Press, 2020.

[34] Y. Xing, E. W. M. Ma, K. L. Tsui *et al.*, "Battery management systems in electric and hybrid vehicles," *Energies*, vol. 4, no. 11, pp. 1840–1857, 2011.

[35] T. Stuart, F. Fang, X. Wang *et al.*, "A modular battery management system for hevs," *SAE Transactions*, pp. 777–785, 2002.

[36] D. Andrea, *Battery management systems for large lithium-ion battery packs*. Artech House, 2010.

[37] E. Meissner and G. Richter, "Battery monitoring and electrical energy management: Precondition for future vehicle electric power systems," *Journal of Power Sources*, vol. 116, no. 1-2, pp. 79–98, 2003.

[38] J. D. Kozlowski, "Electrochemical cell prognostics using online impedance measurements and model-based data fusion techniques," in *2003 IEEE Aerospace Conference Proceedings*, vol. 7, 2003, pp. 3257–3270.

[39] N. A. Windarko, J. Choi, and G. B. Chung, "Soc estimation of lipb batteries using extended kalman filter based on high accuracy electrical model," in *8th International Conference on Power Electronics-ECCE Asia*, 2011, pp. 2015–2022.

[40] A. T. Stamps, C. E. Holland, R. E. White *et al.*, "Analysis of capacity fade in a lithium ion battery," *Journal of Power Sources*, vol. 150, pp. 229–239, 2005.

[41] J. Cao, N. Schofield, and A. Emadi, "Battery balancing methods: A comprehensive review," in *IEEE Vehicle Power Propulsion Conference (VPPC 2008)*, 2008, pp. 1–6.

[42] K. Ng, C. Moo, Y. Chen, and Y. Hsieh, "Enhanced coulomb counting method for estimating state-of-charge and state-of-health of lithium-ion batteries," *Applied Energy*, vol. 86, pp. 1506–1511, 2009.

[43] X. Hu, D. Cao, and B. Egardt, "Condition monitoring in advanced battery management systems: Moving horizon estimation using a reduced electrochemical model," *IEEE/ASME Transactions on Mechatronics*, vol. 23, no. 1, pp. 167–178, 2017.

[44] C. Zhang, J. Jiang, L. Zhang *et al.*, "A generalized soc-ocv model for lithium-ion batteries and the soc estimation for lnmco battery," *Energies*, vol. 9, no. 11, p. 900, 2016.

[45] D. N. How, M. Hannan, M. H. Lipu, and P. J. Ker, "State of charge estimation for lithium-ion batteries using model-based and data-driven methods: A review," *IEEE Access*, vol. 7, pp. 136 116–136 136, 2019.

[46] L. Xing, Y. Mishra, Y.-C. Tian, G. Ledwich, C. Zhou, W. Du, and F. Qian, "Distributed state-of-charge balance control with event-triggered signal transmissions for multiple energy storage systems in smart grid," *IEEE Transactions on Systems, Man, and Cybernetics: Systems*, vol. 49, no. 8, pp. 1601–1611, 2019.

[47] T. Meng, Z. Lin, and Y. A. Shamash, "Distributed cooperative control of battery energy storage systems in DC microgrids," *IEEE/CAA Journal of Automatica Sinica*, vol. 8, no. 3, pp. 606–616, 2021.

[48] W. Huang and J. A. A. Qahouq, "Energy sharing control scheme for state-of-charge balancing of distributed battery energy storage system," *IEEE Transactions on Industrial Electronics*, vol. 62, no. 5, pp. 2764–2776, 2014.

[49] R. Bhosale, R. Gupta, and V. Agarwal, "A novel control strategy to achieve soc balancing for batteries in a dc microgrid without droop control," *IEEE Transactions on Industry Applications*, vol. 57, no. 4, pp. 4196–4206, 2021.

[50] Y. Cao and J. A. A. Qahouq, "Hierarchical soc balancing controller for battery energy storage system," *IEEE Transactions on Industrial Electronics*, vol. 68, no. 10, pp. 9386–9397, 2020.

[51] T. R. Oliveira, W. W. A. G. Silva, and P. F. Donoso-Garcia, "Distributed secondary level control for energy storage management in dc microgrids," *IEEE Transactions on Smart Grid*, vol. 8, no. 6, pp. 2597–2607, 2016.

[52] X. Chen, M. Shi, H. Sun, Y. Li, and H. He, "Distributed cooperative control and stability analysis of multiple dc electric springs in a dc microgrid," *IEEE Transactions on Industrial Electronics*, vol. 65, no. 7, pp. 5611–5622, 2017.

[53] V. Johnson, "Battery performance models in ADVISOR," *Journal of Power Sources*, vol. 110, no. 2, pp. 321–329, 2002.

[54] M. Verbrugge and E. Tate, "Adaptive state of charge algorithm for nickel metal hydride batteries including hysteresis phenomena," *Journal of Power Sources*, vol. 126, no. 1-2, pp. 236–249, 2004.